8-15-1993

Distributions of Pigments and Primary Production in a Gulf-Stream Meander

Steven E. Lohrenz
University of Southern Mississippi

John J. Cullen
Bigelow Laboratory for Ocean Sciences

David A. Phinney
Bigelow Laboratory for Ocean Sciences

Donald B. Olson
University of Miami

Charles S. Yentsch
Bigelow Laboratory for Ocean Sciences

JOURNAL OF GEOPHYSICAL RESEARCH, VOL. 98, NO. C8, PAGES 14,545–14,560, AUGUST 15, 1993

Distributions of Pigments and Primary Production in a Gulf Stream Meander

STEVEN E. LOHRENZ,[1] JOHN J. CULLEN,[2,3] DAVID A. PHINNEY,[2] DONALD B. OLSON,[4] AND CHARLES S. YENTSCH[2]

An investigation was made of physical effects of Gulf Stream meandering on the vertical and horizontal distributions of photosynthetic pigments and primary production. Cruises were conducted in the vicinity of a meander east of 73°W and north of 37°N from September 21 to October 5 (leg 1) and October 12–21, 1988 (leg 2), on the R/V *Cape Hatteras*. Relationships of photosynthesis (normalized to chlorophyll) to irradiance (*P-I*) did not show large horizontal variation, and water column composite *P-I* curves from leg 1 and leg 2 were similar. Therefore a single *P-I* curve derived from pooled data was used to model distributions of primary production. Distributions of photosynthetic pigments were characterized on the basis of in vivo fluorescence profiles and empirical relationships with extracted pigment concentrations. Subsurface irradiance was described using a spectral irradiance model. Cross sections of the Gulf Stream revealed consistently higher pigment concentrations and primary production on the slope water side. Along-stream variations in pigment distributions and primary production were apparently related to density structure influenced by meander circulation. Such variations were less pronounced during leg 2, which came after a transition from a well-defined meander interacting with a warm-core ring (leg 1) to a more linear stream (leg 2). Higher water-column-integrated primary production during leg 2 was attributed to mixing-induced nutrient injection and redistribution of chlorophyll in the photic zone.

INTRODUCTION

Mesoscale features of Gulf Stream circulation have been recognized as important in influencing phytoplankton biomass and primary production distributions [e.g., *Yentsch*, 1987]. Numerous studies of Gulf Stream rings have shown close coupling of biomass and production with physical dynamics of the rings [*Fryxell et al.*, 1985; *Hitchcock et al.*, 1987; *Nelson et al.*, 1985; *Smith and Baker*, 1985; *McCarthy and Nevins*, 1986; Hitchcock et al., 1975], and ring events provide a mechanism for cross-stream exchange among slope and Sargasso Sea water species communities [e.g., *Ortner et al.*, 1978; *The Ring Group*, 1981; *Fryxell et al.*, 1985; *Gould and Fryxell*, 1988]. Other investigations have examined frontal distributions associated with the western edge of the stream which can cause upwelling and intrusion of upwelled water onto the southeastern U.S. continental shelf [e.g., *Atkinson*, 1977; *Lee et al.*, 1981]. When present, such features are believed to dominate processes affecting primary production on the outer shelf [*Yoder et al.*, 1985; *Lee et al.*, 1991].

An aspect of Gulf Stream circulation whose influence on biological parameters is less well studied are meanders occurring offshore east of Cape Hatteras. Meanders, from which rings may develop, are a common circulation feature as the stream branches eastward from the continental shelf. The physical mechanisms influencing biological distributions within these offshore meanders differ from the topographically constrained frontal distributions which occur farther upstream along the shelf break. *Bower and Rossby* [1989] demonstrated that significant vertical and cross-stream circulation can be associated with Gulf Stream meanders. The Biological Synoptic Ocean Prediction (BIOSYNOP) program was an interdisciplinary effort to study biological features of the Gulf Stream front and their response to physical processes associated with meandering of the Gulf Stream [*Olson*, 1990]. These physical processes include vertical mixing, upwelling in the vicinity of the meander crest, downwelling in the trough, and cross-stream exchange. *Flierl and Davis* [1991] presented a model of biological effects of Gulf Stream meandering. *Hitchcock et al.* [1993] described a strong coherence between pigament fields and physical parameters about the meander and suggested that mesoscale chlorophyll distributions were controlled by meander physical processes. Here we present results from cruises conducted in fall 1988 that describe observed patterns of pigments and primary production in relation to the physical structure of a meander. We examined the hypotheses that (1) differences in photosynthetic parameters of phytoplankton populations were related to different physical regimes within the meander and the associated water masses and (2) along-stream variations in distributions of pigments and primary production could be related to meander physical structure.

METHODS

Sampling was performed aboard the R/V *Cape Hatteras* from September 21 to October 4 (leg 1) and October 11–20, 1988 (leg 2). Station data are given in Table 1. For each leg an initial mesoscale survey was performed consisting of vertical stations transecting the Gulf Stream (Plates 1 and 2). This was followed by additional sampling at selected locations (Table 1). Positions of stations in relation to the Gulf Stream were guided by advanced very high resolution radiometer (AVHRR) imagery (e.g., Plates 1 and 2) and expendable bathythermograph data (not shown). Conductivity/temperature/depth (Seabird SBE 9 underwater unit with SBE 11 deck unit) and in situ fluorescence (SeaTech) profiles

[1]Center for Marine Science, University of Southern Mississippi, Stennis Space Center.
[2]Bigelow Laboratory for Ocean Sciences, West Boothbay Harbor, Maine.
[3]Now at Department of Oceanography, Dalhousie University, Halifax, Nova Scotia, Canada.
[4]Rosenstiel School of Marine and Atmospheric Sciences, University of Miami, Miami, Florida.

Paper number 93JC00678.
0148-0227/93/93JC-00678$05.00

TABLE 1. Station Location Data, Curvilinear Coordinates and Integrated Water Column Pigment and Production Estimates for Stations Occupied During R/V *Cape Hatteras* Cruises CH08-88 (Leg 1) and CH09-88 (Leg 2)

Station	Date	UT	Latitude, °N	Longitude, °W	Curvilinear Coordinates,* km		Integrated Pigments, g m^{-2}	Integrated Production, gC m^{-2} d^{-1}	Parameters†
					Along-Stream	Cross-Stream			
					Leg 1				
2	Sept.21	1021:51	37.599	73.200	−141.40	95.76	0.054	0.60	pg, *n*, *SIS*
3	Sept.21	1626:59	37.548	72.934	−141.98	74.36	0.070	0.65	
4	Sept.21	2037:53	37.501	72.663	−140.99	50.04	0.085	0.59	pg, *n*, *SIS*
5	Sept.22	0140:19	37.450	72.414	−142.68	28.19	0.063	0.56	
6	Sept.22	0659:03	37.376	71.988	−144.60	−8.57	0.038	0.40	pg, *n*, *SIS*
7	Sept.22	1250:26	37.660	71.976	−114.17	9.90	0.041	0.45	
8	Sept.22	2216:31	37.879	72.000	−106.67	30.35	0.060	0.56	pg, *n*, *SIS*
9	Sept.23	0356:52	38.117	72.001	−90.56	49.71	0.085	0.75	
10	Sept.23	0910:43	37.921	71.744	−93.21	18.31	0.051	0.48	pg, *n*, *SIS*
11	Sept.23	1714:09	37.735	71.500	−94.89	−10.65	0.047	0.36	pg, *SIS*
12	Sept.24	0204:04	37.553	71.250	−91.10	−38.44	0.056	0.38	pg, *n*
13	Sept.24	1016:58	37.698	70.914	−48.15	−40.47	0.048	0.36	
14	Sept.24	1920:48	37.902	70.609	−9.66	−27.85	0.046	0.36	pg, *n*, *SIS*
15	Sept.25	0154:47	38.066	70.295	28.02	−3.36	0.045	0.38	
16	Sept.25	0942:36	38.182	70.079	34.59	16.85	0.079	0.53	pg, *n*, *SIS*
17	Sept.25	1549:23	38.319	69.865	35.08	40.12	0.067	0.57	
18	Sept.25	1924:57	38.316	69.864	33.70	39.65	0.077	0.62	pg, *n*, *SIS*
19	Sept.25	2229:12	38.056	69.862	50.07	17.15	0.080	0.48	
20	Sept.26	1118:17	37.653	68.885	130.04	53.64	0.061	0.49	pg, *n*, *SIS*
21	Sept.26	1751:16	37.613	69.310	112.12	17.69	0.081	0.40	pg, *n*, *SIS*
22	Sept.27	0404:34	37.686	69.860	74.80	−18.01	0.038	0.38	pg, *n*, *SIS*
23	Sept.27	1126:34	38.067	69.862	38.40	9.40	0.043	0.37	
24	Sept.27	1218:32	38.096	69.784	44.80	14.98	0.065	0.42	pg, *n*, *SIS*
25	Sept.28	1236:26	37.319	71.902	−184.40	29.73	0.075	0.45	
26	Sept.28	1529:48	37.238	72.066	−186.60	44.38	0.059	0.39	
27	Sept.28	1744:58	37.441	72.198	−181.83	60.19	0.083	0.56	
28	Sept.28	1847:59	37.443	72.182	−181.90	60.86	0.061	0.54	
29	Sept.29	1005:56	37.237	72.020	−178.11	36.26	0.061	0.37	pg, *n*, *SIS*
30	Sept.29	2222:30	38.019	71.199	−74.18	14.96	0.060	0.51	
31	Sept.30	0049:29	38.159	71.468	−82.50	38.10	0.062	0.64	
32	Sept.30	0534:02	38.172	71.073	−55.50	28.47	0.055	0.58	
33	Sept.30	1134:58	37.957	.287	−96.50	26.09	0.067	0.64	pg, *n*, *SIS*
34	Oct. 1	1811:54	37.970	70.754	−92.90	7.96	0.061	0.36	pg, *n*, *SIS*
35	Oct. 1	1854:44	37.994	70.701	−91.90	6.85	0.042	0.37	
36	Oct. 2	1007:26	37.891	70.915	−104.60	15.80	0.059	0.42	pg, *n*, *SIS*
37	Oct. 2	1120:11	37.883	70.934	−104.20	18.51	0.050	0.43	
38	Oct. 2	2245:20	37.716	70.024	−56.20	−51.23	0.042	0.35	
39	Oct. 3	1722:13	37.814	69.044	87.10	18.56	0.062	0.37	pg, *n*, *SIS*
					Leg 2				
42	Oct.12	0125:58	37.702	70.730	−128.80	26.40	0.120	0.76	pg, *n*
43	Oct.12	0444:35	37.628	70.525	−116.60	11.23	0.070	0.46	
44	Oct.12	1209:09	37.534	70.400	−118.40	0.32	0.050	0.43	pg, *n*, *P-I*
45	Oct.12	1746:48	37.749	69.999	−75.30	13.14	0.058	0.41	*P-I*
46	Oct.13	2352:35	37.917	70.132	−91.40	36.50	0.075	0.66	pg, *n*
47	Oct.13	0424:23	38.104	70.002	−65.80	51.57	0.061	0.69	
48	Oct.13	1146:06	38.070	69.658	−49.80	36.19	0.063	0.59	pg, *n*, *P-I*
49	Oct.13	1410:31	37.919	69.528	−50.10	17.42	0.060	0.51	pg, *n*, *P-I*
50	Oct.13	2111:48	37.751	69.243	−33.70	−4.56	0.041	0.44	
51	Oct.14	0219:35	37.996	69.116	−27.80	22.30	0.072	0.62	
52	Oct.14	0638:15	38.164	69.113	−32.90	41.76	0.065	0.67	
53	Oct.14	1352:12	38.250	68.834	−8.83	52.32	0.067	0.69	pg, *n*, *P-I*
54	Oct.14	1650:08	38.077	68.490	8.33	36.02	0.080	0.69	pg, *n*, *P-I*
55	Oct.14	2244:41	37.968	68.603	1.35	22.27	0.050	0.52	
56	Oct.15	0355:49	37.843	68.678	0.00	7.16	0.042	0.49	*n*
57	Oct.15	1159:57	37.677	68.723	−6.77	−9.19	0.037	0.41	pg, *P-I*
58	Oct.15	1657:26	37.613	68.668	−1.77	−16.32	0.032	0.36	*P-I*
59	Oct.16	0230:52	34.082	67.749	73.10	55.32	0.077	0.85	
60	Oct.16	0822:39	37.811	67.816	80.10	23.83	0.064	0.52	
61	Oct.16	1157:44	37.662	67.814	93.55	7.78	0.039	0.38	pg, *n*, *P-I*
62	Oct.16	1715:31	37.483	67.904	96.84	−13.55	0.038	0.34	pg, *n*, *P-I*
63	Oct.16	2205:05	37.808	68.067	85.47	19.44	0.050	0.44	
64	Oct.17	0857:08	37.596	68.738	51.92	−9.72	0.032	0.40	pg
65	Oct.17	1248:60	37.609	68.470	82.60	−6.54	0.033	0.40	*P-I*
66	Oct.17	1613:42	37.611	68.256	112.90	−3.09	0.040	0.37	*n*, *P-I*
67	Oct.17	1943:32	37.610	68.045	135.90	−2.03	0.038	0.40	*P-I*
68	Oct.18	1728:07	37.620	69.787	−21.60	−8.39	0.045	0.35	pg, *n*, *P-I*

TABLE 1. (continued)

Station	Date	UT	Latitude, °N	Longitude, °W	Curvilinear Coordinates,* km: Along-Stream	Curvilinear Coordinates,* km: Cross-Stream	Integrated Pigments, g m^{-2}	Integrated Production, gC m^{-2} d^{-1}	Parameters†
					Leg 2				
69	Oct.19	0110:56	37.773	70.420	−73.80	19.99	0.072	0.64	
70	Oct.19	0841:29	37.664	69.901	−29.50	−4.20	0.043	0.48	pg
71	Oct.19	1306:15	37.637	69.475	10.10	−9.56	0.037	0.49	*P-I*
72	Oct.19	1606:48	37.642	69.181	38.50	−4.55	0.046	0.49	*n*, *P-I*
73	Oct.19	2300:52	37.662	68.564	85.30	10.75	0.046	0.54	
74	Oct.20	0110:17	37.754	68.521	85.30	21.99	0.061	0.63	

*Curvilinear coordinate system for the meander as described by *Mariano* [1990, 1991]. The nominal cross-stream coordinate of the high velocity core is 0 km and the north wall of the Gulf Stream is usually located between 20 and 25 km. The along-stream coordinate of the meander crest is 0 km with positive values corresponding to the downstream direction.

†Conductivity/temperature/depth and fluorometry were measured at all stations. Other parameters were as follows: pg, pigments; *n* nutrients; *SIS*, simulated in situ primary production; *P-I*, photosynthesis-irradiance.

were obtained at all stations. Fluorometric assays of photosynthetic pigments (modified from *Holm-Hansen et al.* [1965]) were performed at selected stations (Table 1). Concentrations of chlorophyll *a* (Chl *a*) and phaeopigments were determined fluorometrically using a Turner Designs 10-005R fluorometer fitted with a Corning 5-60 excitation filter and a 2-64 emission filter. Samples were filtered on glass fiber (Whatman GF/F) filters and extracted in 10 mL of 90% acetone in darkness for at least 24 hours at −4°C. The fluorometer was calibrated with purified Chl *a* for leg 1. For leg 2, calibrations were made using extracts from laboratory cultures for which the Chl *a* concentration had been determined spectrophotometrically [e.g., *Parsons et al.*, 1984]. At selected stations (Table 1), nutrient samples from the surface mixed layer were preserved and subsequently analyzed on shore by chemiluminescent assay for nitrate + nitrite [*Garside*, 1982]. Deeper samples were frozen and subsequently analyzed on shore by autoanalyzer (Technicon) following procedures of *Whitledge et al.* [1981].

Primary Production and Photosynthesis-Irradiance Measurements

Primary production during leg 1 was determined by in situ and simulated in situ methods. Short term (<1 hour) in situ primary production measurements were determined at stations 33 (15 m) and 34 (15, 45, and 75 m) using an autonomous submersible sampling and incubation device (*Taylor and Doherty* [1990], as described by *Lohrenz et al.* [1992]). Primary production was determined by the simulated in situ method at selected stations (Table 1) generally at six depths throughout the photic zone. Samples for simulated in situ incubations were collected using acid-cleaned Niskin bottles with silicon rubber O-rings and cap springs. Subsamples were placed in acid-cleaned 0.25-L polycarbonate bottles, and $NaH^{14}CO_3^-$ was added to a final concentration of 0.1 mCi L^{-1}. The total added activity was determined by the addition of a 50-μL aliquot of sample in 4-mL Scintiverse II scintillation fluor plus 50-μL phenethylamine, 50-μL 1 *M* Tris (hydroxymethyl) aminomethane HCl, and 100-μL Milli-Q deionized water. Replicate bottles were incubated for 4–8 hours and for 24 hours under simulated in situ conditions in temperature-controlled and spectrally adjusted deck incubators [*Lohrenz et al.*, 1988, 1992]. Incubation irradiance was adjusted to correspond to in situ levels. The percentage of surface irradiance in the incubators was determined by measurements obtained with a Biospherical Instruments QSL-100. Irradiance measurements were obtained at various positions within the tanks and over a representative range of solar zenith angles. Mean coefficient of variation of irradiance as a function of location within the tanks was 22% (range of 0.7–70%). After incubation, samples were filtered onto glass fiber filters (Whatman GF/F) using gentle vacuum (<100 mm Hg), and filters were acidified with 0.5 mL 1 *N* HCl to eliminate inorganic ^{14}C [*Lean and Burnison*, 1979]. Activities of productivity samples were determined by liquid scintillation analysis (Packard Tri-Carb 2000CA). Liquid scintillation counts were corrected for quenching by the channels ratio method. Final values were corrected for zero-time activities. No correction was made for isotope discrimination. Total dissolved inorganic carbon samples for specific activity calculations were collected in serum stoppered bottles and preserved with sodium azide (final concentration of 0.001 *M*). Acid-volatilized CO_2 concentrations were determined by infrared absorption spectroscopy (Horriba).

During leg 2 at selected stations (Table 1), photosynthesis as a function of irradiance (*P-I*) was determined using a modification of the method of *Lewis and Smith* [1983]. Generally, measurements were made at four depths. Samples were inoculated with $NaH^{14}CO_3^-$ (final concentration, 10 mCi L^{-1}) and aliquots of 1 mL were dispensed into glass scintillation vials (7-mL capacity) in a temperature-controlled aluminum block. Total added activity was determined by subsampling into 5-mL Ecolume scintillation fluor plus 0.2-mL phenethylamine. A range of "white" irradiance was provided with 2 ENH-type tungsten-halogen projection lamps directed through a heat filter of circulating water and attenuated with neutral density screens. Quantum scalar irradiance in each position was measured with a Biospherical Instruments QSL-100 4π sensor with a collector modified to fit in the bottom half of a scintillation vial for the measurements. Incubations began within 30 min of sampling and were terminated after 1 hour. Inorganic carbon was expelled by adding 0.5 mL 6 *N* HCl and agitating the open vials for at least 1 hour in a hood. Ecolume scintillation fluor was added, and the vials were agitated again before scintillation counting. Total dissolved inorganic carbon was assumed to be 2.1

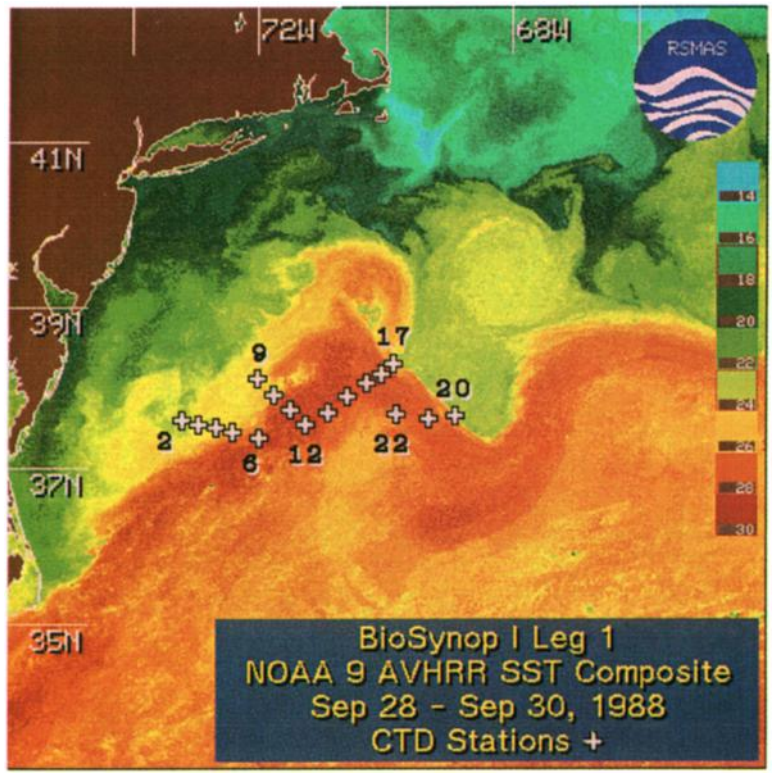

Plate 1. National Oceanic and Atmospheric Administration (NOAA 9) advanced very high resolution radiometer (AVHRR) image of sea surface temperature on September 28–30, 1988. Data for vertical sections across the Gulf Stream core (see Figures 7 and 8) were obtained from vertical stations indicated by crosses. Locations of these and additional stations are provided in Table 1.

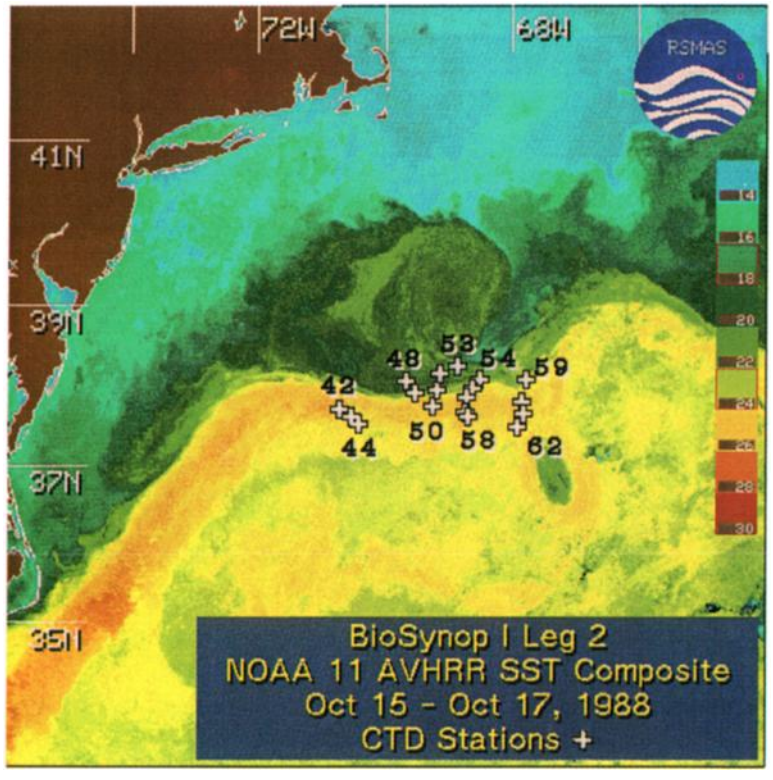

Plate 2. NOAA 9 AVHRR image of sea surface temperature on October 15–17, 1988. Data for vertical sections across the Gulf Stream core (see Figure 9) were obtained from vertical stations indicated by crosses. Locations of these and additional stations are provided in Table 1.

mM, a value comparable to the mean photic zone concentration of 2.20 ± 0.08 (N = 23) determined during leg 1.

The *P-I* equation of *Platt et al.* [1980] was used to model the results:

$$P = B\ P_s^B[1 - \exp(-\alpha^B I/P_s^B)]\,[\exp(-\beta^B I/P_s^B)] \quad (1)$$

where P (mg C m^{-3} h^{-1}) is the primary production rate, B (mg Chl a m^{-3}) is the biomass concentration, P_s^B (g C g Chl a^{-1} h^{-1}) is the saturated rate of Chl a-normalized photosynthesis in the absence of photoinhibition, α^B (g C g Chl a^{-1} h^{-1} (μmol quanta m^{-2} s^{-1})$^{-1}$) is the initial slope of the *P-I* curve, β^B (g C g Chl a^{-1} h^{-1} (μmol quanta m^{-2} s^{-1})$^{-1}$) is the parameter to characterize photoinhibition, and I (μmol quanta m^{-2} s^{-1}) is the available quantum scalar irradiance. Parameters were fit simultaneously using the NLIN procedure of SAS. An intercept P_0^B (g C g Chl a^{-1} h^{-1}) was included as a parameter and subsequently subtracted from estimates of P as one would do with a zero-time value. The inclusion of P_0^B increases the amount of explained variability and improves the distribution of residuals. By subtracting rather than including P_0^B from estimates of P, the modeled photosynthesis in the dark is always zero. The maximum photosynthetic rate $P_{\max}^B$ can be computed from the following equation [*Platt et al.*, 1980]:

$$P_{\max}^B = P_s^B[\alpha/(\alpha + \beta)]\,[\beta/(\alpha + \beta)]^{\alpha/\beta} \quad (2)$$

For simplicity of notation the B superscripts have been dropped in this and subsequent references to α and β. Note that as β approaches zero, $P_{\max}^B$ approaches P_s^B.

Estimation of Pigment and Chlorophyll Concentrations From in Situ Fluorescence

To better complement scales of physical measurements, we extended the vertical and areal resolution of discrete analyses of Chl a and total pigments (Chl a and phaeopigments) using empirical relationships with in situ fluorescence ($F_{\text{in situ}}$). Profiles of $F_{\text{in situ}}$ were obtained routinely at all stations. The development of an empirical model to estimate concentrations of total pigments from $F_{\text{in situ}}$ provided more detailed characterization of pigment distributions; the modeled pigment distributions were also used as input for the computation of subsurface irradiance as described below. Similarly, an empirical model to estimate concentrations of Chl a from $F_{\text{in situ}}$ was used to provide input for the biomass term in (1) when modeling distributions of primary production. To develop these empirical models, we used a stepwise multiple regression routine (Systat) to determine the utility of the variables $F_{\text{in situ}}$ (volts), depth (meters), and time of day as predictors of Chl a and total pigments. Inclusion of time of day as a variable did not significantly improve the models in either case, and depth was a significant predictor only in the case of Chl a. The following relationships were determined:

$$\text{Total pigments (mg m}^{-3}) = 1.12 \pm 0.04[F_{\text{in situ}}] - 0.0539 \pm 0.0166 \quad \text{(model 2 regression, } r^2 = 0.80,\ N = 193) \quad (3)$$

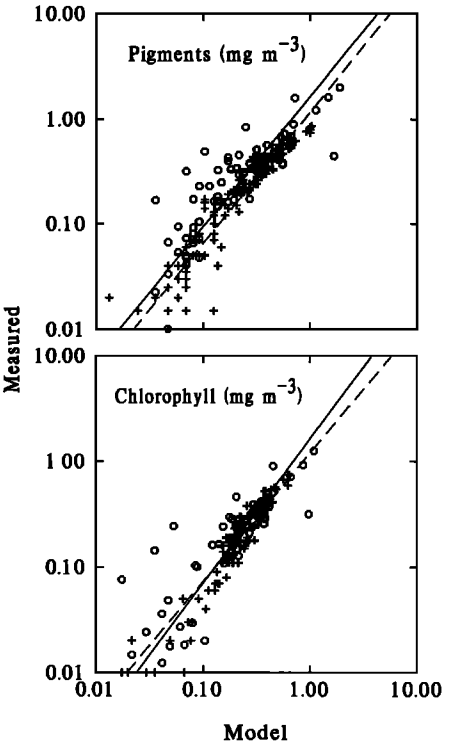

Fig. 1. Comparison of measured total pigments and chlorophyll a (Chl a) concentrations with estimates from empirical models described in methods section. Different symbols designate data from leg 1 (open circles) and leg 2 (crosses). For total pigments, model 2 regressions of $\log_e$-transformed data were as follows: leg 1 (solid line), $\log_e$ (measured pigments) = 1.24 ± 0.08 [$\log_e$ (modeled pigments)] + 0.496 ± 0.150, N = 76, r^2 = 0.72, $p < 0.001$; leg 2 (dotted line), $\log_e$ (measured pigments) = 1.26 ± 0.04 [$\log_e$ (modeled pigments)] + 0.152 ± 0.068, N = 117, r^2 = 0.90, $p < 0.001$. For Chl a, model 2 regressions of $\log_e$-transformed data were as follows: leg 1 (solid line), $\log_e$ (measured Chl a) = 1.36 ± 0.10 [$\log_e$ (modeled Chl a)] + 0.481 ± 0.202, N = 67, r^2 = 0.64, $p < 0.001$; leg 2 (dashed line), $\log_e$(measured Chl a = 1.21 ± 0.40[$\log_e$ (modeled Chl a)] + 0.169 ± 0.090, N = 109, r^2 = 0.88, $p < 0.001$. Coefficient errors are one standard error.

$$\text{Chl } a \text{ (mg m}^3 = 0.596 \pm 0.027(F_{\text{in situ}}) - 0.000513 \pm 0.000074(\text{depth}) + 0.0723 \pm 0.015 \quad (4)$$

$$(r^2 = 0.83,\ N = 193)$$

An analysis of covariance was performed (Systat) to evaluate whether the relationships between modeled and measured values differed between leg 1 and leg 2. Pigment and Chl a concentrations estimated from (3) and (4) were compared to measured values using model 2 regressions of $\log_e$-transformed data (Figure 1). Differences between leg 1 and leg 2 Chl a regression lines were not significant (p = 0.504). In the case of total pigments there was a significant difference between leg 1 and leg 2 regressions of $\log_e$-transformed measured versus modeled data ($p < 0.001$); the difference between adjusted means (expressed as untransformed values) was 26%. This difference was comparable to the mean percent deviation between model estimates and measured values of pigment concentration for each leg; these means were 54% (29% for data above 200 m) for leg 1 and 24% (12% for data above 200 m) for leg 2. Therefore no attempt was made to adjust (3) for differences between leg 1 and leg 2.

Irradiance Models

Continuous measurements of surface incident quantum scalar irradiance $I(0^+)$ were obtained with a Biospherical Instruments QSR-240 solar reference sensor. Surface incident spectral irradiance $I(\lambda, 0^+)$ was approximated using the clear sky irradiance model of *Gregg and Carder* [1990] and scaled such that summation of $I(\lambda, 0^+)$ for wavelengths from 400 to 700 nm was equivalent to measured $I(0^+)$. The model required input of atmospheric properties. The following constants were used: pressure of 1013.25 mbar, relative humidity of 80%, precipitable water vapor of 1.5 cm, and visibility of 15 km. Climatological ozone values were determined using the empirical climatological expression of *Van Heuklon* [1979]. A type 1 air mass (marine aerosols) was assumed.

Scaled values of $I(\lambda, 0^+)$ were used for computations of subsurface in situ quantum scalar irradiance $I(z)$. Initially, spectral irradiance immediately below the sea surface ($I(\lambda, 0^-)$) was computed by adjusted $I(\lambda, 0^+)$ for surface reflectance. Surface reflectance was estimated based on an empirical relationship with wind speed given by *Gregg and Carder* [1990]. We assumed nominal values of 4 m s^{-1} for the mean wind speed and 6 m s^{-1} for the instantaneous wind speed. The estimated proportion of $I(0^+)$ that was reflected at the sea surface was in all cases less than 10%. Subsurface spectral irradiance $I(\lambda, z)$ was computed using a spectral attenuation model [*Lohrenz et al.*, 1992] modified from that described by *Sathyendranath and Platt* [1988]. Modifications included omission of angular distribution terms and use of the expression of *Prieur and Sathyendranath* [1981] to calculate pigment absorption at 440 nm in place of the expression given by *Sathyendranath and Platt* [1988]. Total pigment concentrations were estimated from (3). A 440-nm absorption coefficient for dissolved substances of 0.01 m^{-1} was assumed [cf. Kirk, 1983]. Values of $I(z)$ were computed by summation of $I(\lambda, z)$ from 400 to 700 nm.

To illustrate the validity of this approach, we compared modeled estimates of the attenuation coefficient for downwelling photosynthetically active radiation ($K_d(z)$, m^{-1}) with direct measurements of $K_d(z)$ made using a Li-Cor LI-192SA underwater quantum sensor with LI-190SA surface reference sensor at selected stations (Figure 2). $K_d(z)$ was computed at 2-m depth intervals from the modeled spectral irradiance as follows:

$$K_d(z) = \ln\left[\sum_{\lambda=400}^{700} I(\lambda, z_{i-1})\Delta\lambda \Big/ \sum_{\lambda=400}^{700} I(\lambda, z_i)\Delta\lambda\right] \Big/ (z_i - z_{i-1}) \quad (5)$$

where $I(\lambda, z_i)$ is the spectral irradiance at wavelength λ and depth z_i.

RESULTS

Spatial Variations in Photosynthesis-Irradiance Properties

Spatial variability in photosynthesis-irradiance (P-I) parameters was examined by plotting data as a function of distances either across or along the Gulf Stream (Figure 3).

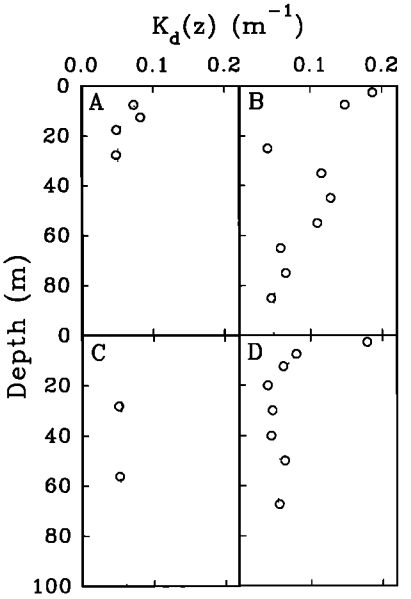

Fig. 2. Comparison of measured (open circles) profiles of the vertical attenuation coefficient [$K_d(z)$] with profiles estimated (dotted lines) using the spectral irradiance attenuation model at four locations, (*a*) station 11, (*b*) station 27, (*c*) station 34), and (*d*) station 36.

Cross-stream and along-stream coordinates corresponded to a curvilinear coordinate system [*Mariano*, 1990, 1991] (Table 1). In the upper mixed layer, highest values of P^B_{max} were encountered in the slope water beyond the north wall of the Gulf Stream (i.e., cross-section coordinates greater than 20–25 km) and near the meander crest (i.e., along-stream coordinate of 0 km). However, the ranges of values overlapped in both cross-stream and along-stream directions. For samples at or below the pycnocline, values of P^B_{max} were consistently lower than upper mixed layer values with no apparent cross-stream or along-stream trends. Highest values of α were observed at or below the pycnocline. The higher values of α and lower values of P^B_{max} in the deeper samples would be expected for low light-adapted populations [cf. *Harrison et al.*, 1985]. Although values of α at or below the pycnocline were generally higher than those in the mixed layer, there were instances where the ranges of values overlapped. Specifically, overlap occurred where a wide range of values of α from deep samples was encountered at cross-stream coordinates of −5 to −8 km and an along-stream coordinate of approximately 100 km. In addition, there were overlapping ranges of mixed layer and pycnocline values observed in the slope water as a consequence of higher values of α in the mixed layer.

To permit comparisons of photosynthesis-irradiance (P-I) relationships between leg 1 and leg 2, water column composite P-I curves were constructed (Figure 4). Data from the short-term (4–8 hours) production rates determined during leg 1 were normalized to Chl *a* concentrations and plotted versus the incubation irradiance (Figure 4*a*). The pooled data from all depths sampled were fit to equation (1). Because estimates of β and P^B_0 terms were not significantly different from zero, these terms were omitted. For comparison with leg 2 data an analogous composite curve was derived using the leg 2 P-I parameters [cf. *Cullen et al.*,

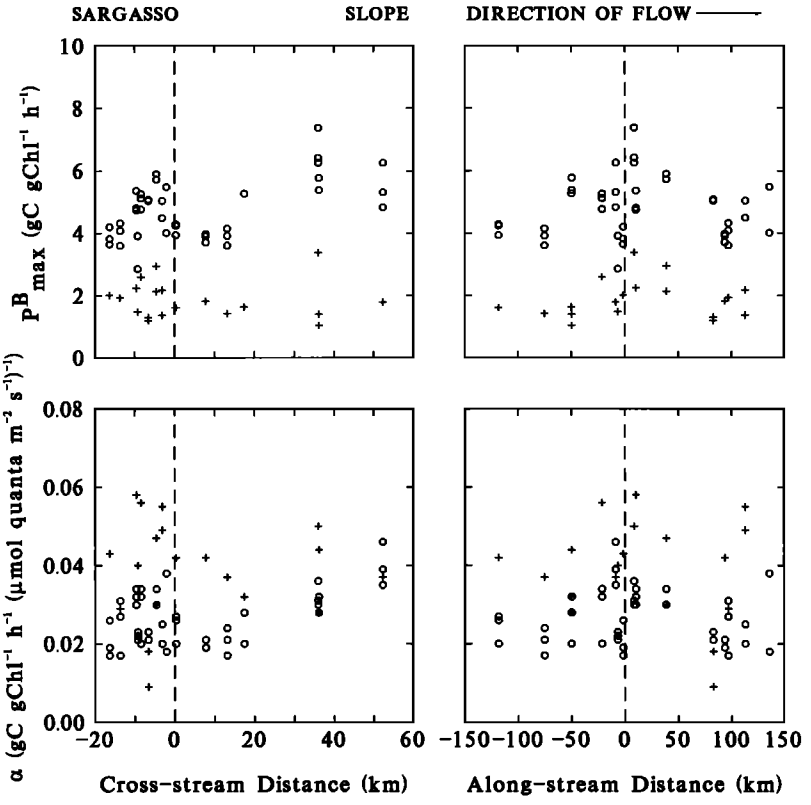

Fig. 3. Photosynthesis-irradiance parameters of phytoplankton populations from the upper mixed layer (open circles) and below the pycnocline (crosses) in relation to positions across and along the Gulf Stream meander. Cross-stream and along-stream distances were those corresponding to a curvilinear coordinate system used for objective analysis mapping [*Mariano*, 1990, 1991]. The nominal cross-stream coordinate of the high-velocity core is 0 km, and the north wall is usually located between 25 and 20 km. The along-stream coordinate of the meander crest is 0 km with positive values corresponding to the downstream direction.

1992]. This was achieved by computing a Chl *a*-normalized photosynthesis rate ($P/B = P^B$) for each set of *P-I* parameters using (1) and the modeled in situ irradiance corresponding to the location, time, and depth of sampling ($I(z)$). The resulting P^B versus $I(z)$ data were fit to (1), with β and P^B_0 terms omitted as above. Despite the observed depth-dependent and spatial variations in P^B_{max} and α (Figure 3), the water column composite photosynthesis-irradiance data from leg 2 were well represented by a single curve (Figure 4*b*). Furthermore, the overlap of coefficient errors for the leg 1 and leg 2 composite curves (Figure 4) indicated that differences were not significant. Consequently, the P^B versus $I(z)$ data from both cruises were pooled and fit to (1) yielding a single *P-I* relationship where $P^B_s = 5.0 \pm 0.2$ g C g Chl a^{-1} h^{-1} and $\alpha = 0.031 \pm 0.3$ g C g Chl a^{-1} h^{-1} (μmol quanta m^{-2} s^{-1})$^{-1}$.

Modeling Primary Production

Production *P* at each depth was estimated from (1) using the above water column composite *P-I* parameters, Chl *a* estimated from (4), and modeled $I(z)$. Modeled estimates of hourly primary production agreed well with in situ measurements made at selected depths at stations 33 and 34 (Figure 5*a*). Profiles of daily primary production were computed using an approach modified from that of *Fee* [1973]. Rates computed for 1-hour intervals were summed over the photoperiod to give daily production at depth increments of approximately 5 m. Measurements of daily production from 24-hour simulated in situ (SIS) incubations were reasonably represented by modeled estimates corresponding to the location, time, and depth of sampling (Figure 5*b*). Some of the scatter in the data in Figure 5*b* may have resulted from errors in the SIS measurements such as, for example, in matching incubation irradiance with in situ levels [cf. *Lohrenz et al.*, 1992] and from effects of long-term sample confinement (see review of SIS method by *Lohrenz* [1993]). Potential limitations of the model must also be recognized. The model tended to underestimate SIS values at low rates and overestimate them at high rates. Reasons for underestimation include the fact that the model assumed a constant value of α when, in fact, α increased with depth (Figure 3). Reasons for overestimation include the fact that the model did not account for losses associated with night respiration. Despite such limitations, trends in measured productivity were well represented by the model as indicated by significant correlations (Figure 5).

The model was used to characterize vertical and areal distributions of primary production. The principal variable input to the model was in situ fluorescence, from which Chl *a* and $I(z)$ were determined as previously described. Input of hourly surface irradiance $I(0^+)$ was also required, and we used the hourly means of $I(0^+)$ measured over the entire study. This was reasonable as the hourly means of $I(0^+)$ measured during leg 1 were not significantly different from

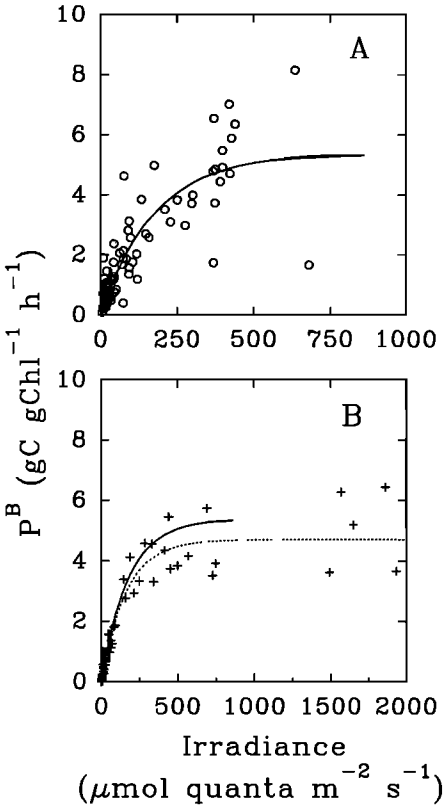

Fig. 4. (*a*) Chlorophyll *a*-specific photosynthesis rates versus quantum scalar irradiance for data from simulated in situ incubations conducted during leg 1. Solid line represents nonlinear least squares fit of leg 1 data to (1). Parameters and standard errors were $P_s^B = 5.4 \pm 0.5$ gC gChl^{-1} h^{-1} and $\alpha = 0.030 \pm 0.004$ gC gChl^{-1} h^{-1} (μmol quanta m^{-2} s^{-1})$^{-1}$; $N = 75$. (*b*) An analogous relationship was derived for leg 2 as described in the text. The dotted line represents a nonlinear least squares fit of leg 2 data to (1). Parameters and standard errors were $P_s^B = 4.7 \pm 0.2$ gC gChl^{-1} h^{-1} and $\alpha = 0.029 \pm 0.003$ gC gChl^{-1} h^{-1} (μmol quanta in m^{-2} s^{-1})$^{-1}$; $N = 61$. Leg 1 fit (solid line) is shown for comparison. Note difference in irradiance scales between Figures 4*a* and 4*b*.

means determined during leg 2 (data not shown). This approach eliminated surface incident irradiance as a source of regional variability and simplified evaluation of spatial differences.

Meander Evolution as Revealed by Sea Surface Temperature

During the leg 1 mesoscale survey, AVHRR imagery (year day (Y.D.) 266, September 24 and Y.D. 267, September 25, 1988) revealed a well-developed meander with a wavelength of approximately 350 km and an amplitude of nearly 100 km (Figure 6). As this meander propagated to the east, it began an interaction with a warm-core, anticyclonic ring (Plate 1). This interaction was accompanied by perturbations in flow on the westward side of the meander and, eventually, by considerable exchange of near-surface waters out of the stream and around the ring. The ring–stream interaction peaked around Y.D. 269–270. The interaction concluded with the formation of a cyclonic, cold-core ring on the eastern side of the meander on Y.D. 287–288 [*Tracey and Watts*, 1990] and with the subsequent collapse of the meander (Plate 2). Velocities in the stream were continuously measured using an acoustic doppler current profiler and the ship's navigation data (results not shown). During the latter part of leg 2, the stream was essentially zonal with higher velocities than observed during the initial portions of the survey. The increased velocities were observed throughout the upper water column.

Cross Sections of Density, Pigments, Primary Production, and Nutrients

Cross sections of the Gulf Stream during mesoscale surveys of the meander revealed some similarities between leg 1 (Figures 7 and 8) and leg 2 (Figure 9). In all cases, sections across the Gulf Stream revealed higher biomass and productivity on the slope water side of the Gulf Stream core. However, along-stream patterns, apparently related to density structure influenced by mesoscale circulation, were different between leg 1 and leg 2. As discussed below, the transition from a nearly constant amplitude meander in interaction with a warm-core ring (Plate 1, leg 1) to a linear stream (Plate 2, leg 2) was associated with a pronounced change in signals observed during the surveys.

Leg 1. During leg 1 the subsurface pigment maximum (coinciding approximately with the $\sigma_t = 25$ isopycnal) was shallowest in the western portion of the anticyclonic meander crest (stations 2–6) (Figure 7). The downstream progression of sections, extending to the cyclonic trough (stations 20–22), revealed progressively deeper subsurface pigment maxima. The nitracline was also deeper in the cyclonic trough (Figure 8). For both legs 1 and 2 we found a close

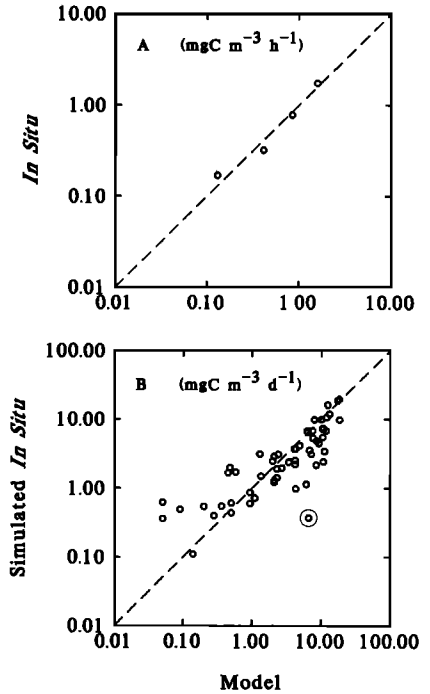

Fig. 5. (*a*) Comparison of hourly primary production estimated by short-term (0.5–1 hour) in situ incubations with modeled estimates ($r^2 = 0.96$; $N = 4$; $p = 0.021$) at stations 33 and 34. Line represents a 1:1 relationship. (*b*) Comparison of daily production estimated by 24-hour simulated in situ incubations with modeled estimates ($r^2 = 0.67$; $N = 57$; $p < 0.001$). Omission of the anomalously low simulated in situ value (circled) resulted in an improved correlation ($r^2 = 0.74$; $N = 56$; $p < 0.001$).

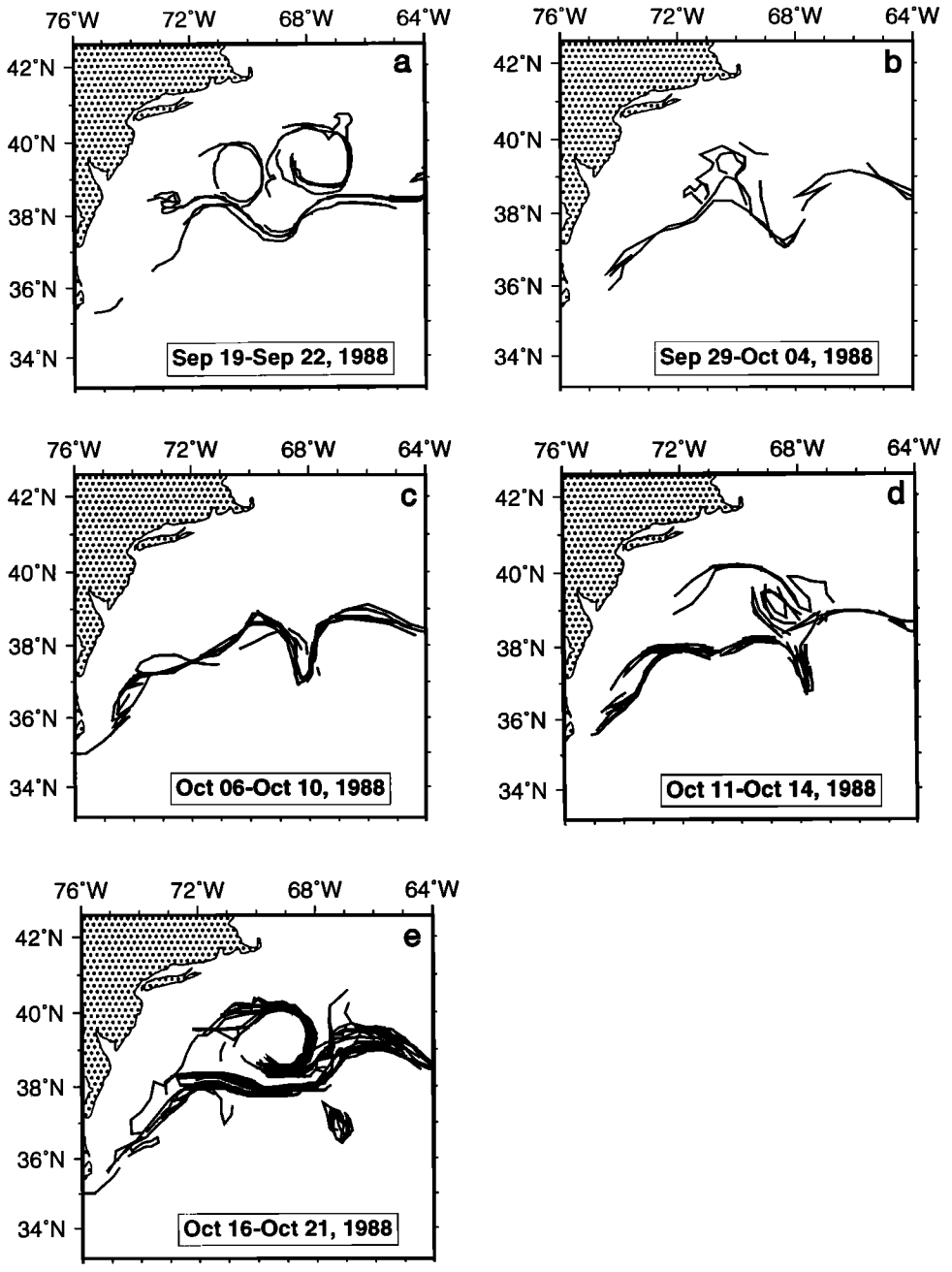

Fig. 6. Analysis of frontal positions (maximum surface temperature gradient) of the Gulf Stream and surrounding ring field. To minimize obscuration by clouds, frontal locations were digitized from composites of AVHRR imagery over the periods listed at the bottom of each frame. (*a*) The analysis period began with a large meander propagating eastward into a warm-core ring. (*b*) The period (September 29 to October 4) revealed a strong interaction between the ring and the meander. (*c*) and (*d*) The subsequent periods depicted the culmination of this interaction and the steepening of a cold meander to the south which eventually formed a cold-core ring. This ring formation event was accompanied by a reduction in the amplitude of the western meander.

relationship between density and $NO_3^- + NO_2^-$ concentrations (Figure 10).

Consistent with the observed distribution of pigments, along-stream variations were evident in vertical distributions of primary production. There was a strong cross-stream gradient in primary production at the western transect (stations 2–6), which became less pronounced in subsequent sections downstream (Figure 7). Rates of primary production were inversely related to the depths of subsurface pigment maxima.

Leg 2. Consistent with observations during leg 1, along-stream variation in the depths of subsurface pigment maxima at the stream core reflected changes in the density field (Figure 9). Depths of the subsurface pigment maxima along the stream core during leg 2 generally varied between 70 and 100 m, smaller than the range of 50–130 m encountered during leg 1. Subsurface pigment maxima along the northern edge of the Gulf Stream were generally less distinct than those observed during leg 1 and, in some cases, extended into the surface mixed layer; surface densities were also

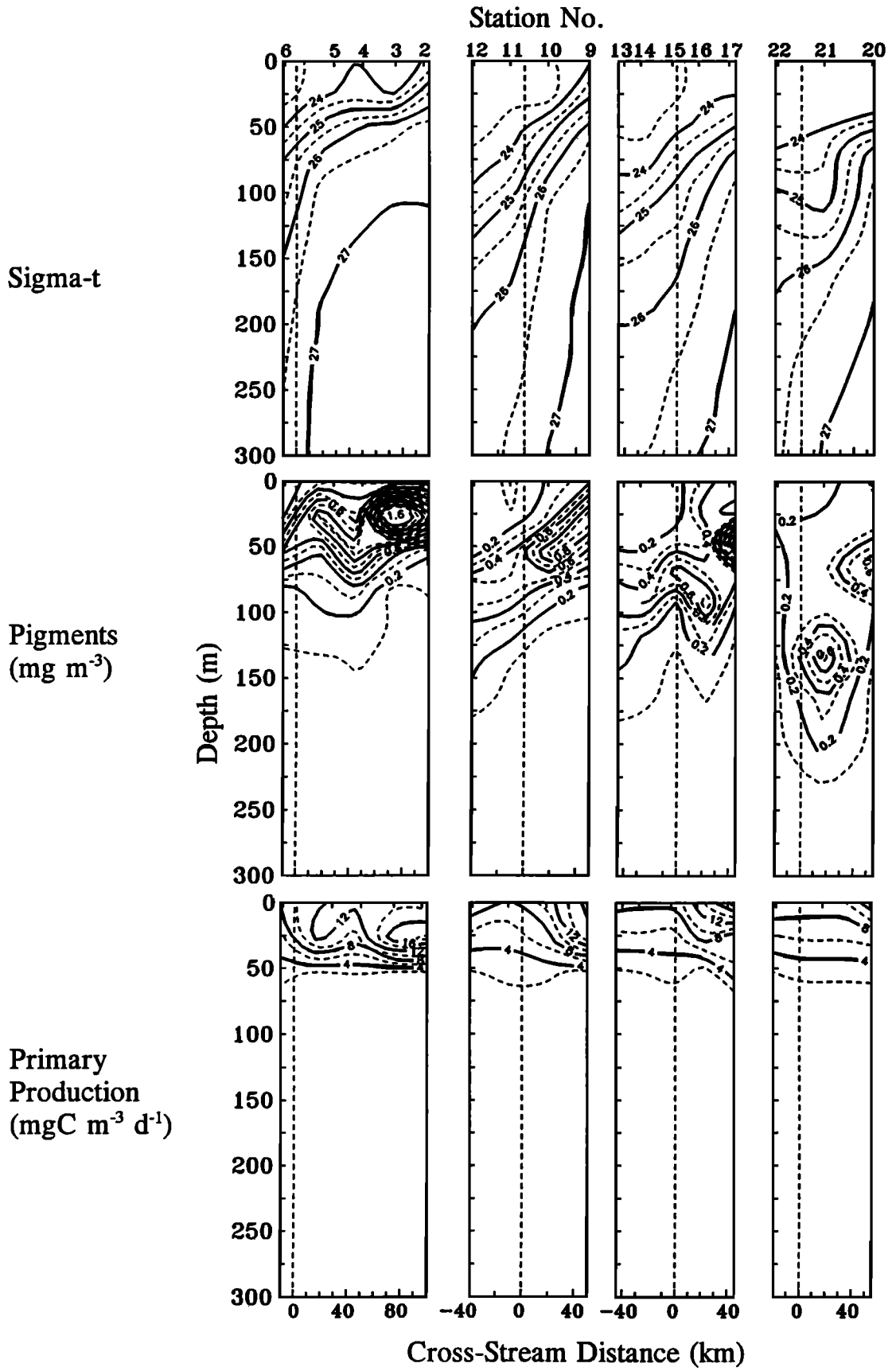

Fig. 7. The σ_t, total pigments, and daily primary production for sections across the Gulf Stream during the leg 1 mesoscale survey. Station numbers are shown along the top. Cross-stream distances were as described in Figure 3. The sequence of sections is in an along-stream progression from the western portion of the anticyclonic meander crest (stations 2–6) to the cyclonic trough (stations 20–22). See Plate 1 for position of transects in relation to meander.

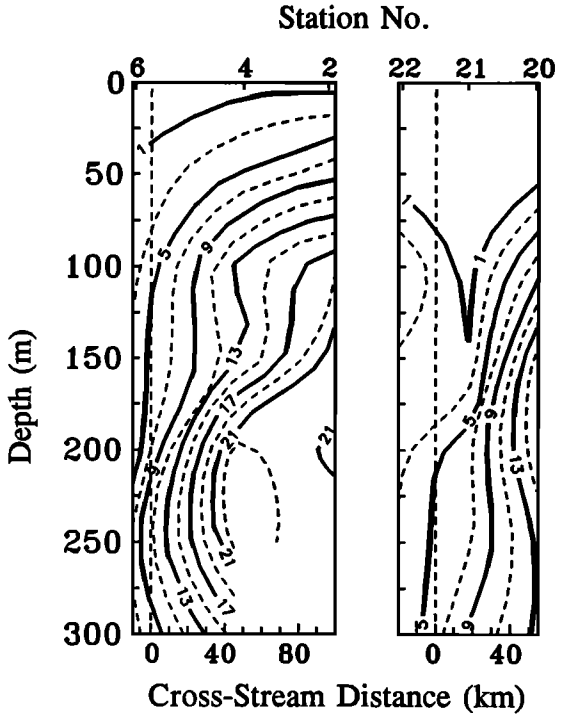

Fig. 8. NO_3^- + NO_2^- (mmol m^{-3}) sections across the Gulf Stream during the leg 1 mesoscale survey. Nutrients were not determined at stations 3 and 5. The nitracline was nominally designated as the 1 mmol m^{-3} isoline. Labeling and notation are as in Figure 7.

generally higher than those observed during leg 1. In addition, during leg 2, near-surface rates of primary production north of the Gulf Stream core reached higher values than those observed during leg 1. To illustrate changes in the water column structure between leg 1 and leg 2, a comparison was made (Figure 11) of vertical profiles of total pigments and density between two locations, stations 8 and 46, occupied during leg 1 and leg 2, respectively, and having similar positions relative to the meander (i.e., similar curvilinear coordinates, see Table 1). A distinct subsurface pigment maximum, apparent at station 8, was not evident at station 46, where the density profile revealed a deeper mixed layer.

Temporal and Spatial Variations in Water-Column-Integrated Pigments and Primary Production

Consistent with cross-section observations, water-column-integrated pigments (Figure 12 and Table 1) and primary production (Figure 13 and Table 1) were consistently higher on the slope water side of the Gulf Stream for both legs 1 and 2. Generally, cross-stream differences exceeded those observed in the along-stream direction. However, some along-stream variations were evident. During leg 1, integrated primary production (Figure 13) was highest in slope water upstream of the crest (along-stream coordinates near −90 km). This coincided with the area where subsurface pigment maxima (Figure 7) and the nitracline (Figure 8) were nearer the surface. Along-stream variations in integrated pigments (Figure 12) were evident during leg 2. The highest concentration of integrated pigments was observed at the northern edge of the stream in the vicinity of the cyclonic trough (along-stream coordinates near −128 km). This location also exhibited relatively high integrated primary production (Figure 13). There was other evidence of along-stream variation in integrated primary production during leg 2, with highest values occurring in the slope water downstream of the crest (along-stream coordinates of 75 km). This corresponded to a region of substantial ring interaction (Figure 6). Water-column-integrated primary production along the stream on the slope water side was uniformly higher during leg 2 as compared with leg 1 (Figure 13), and this was consistent with the patterns observed in near-surface rates of primary production (compare Figures 7 and 9).

In modeling primary production during this study we assumed that a single set of parameters was representative of all regions at all times during the study. As described previously, this assumption was based on evaluations of parameters that included coefficients for estimating total pigments and Chl *a* concentrations from in situ fluorescence profiles (equations (3) and (4)) and the parameters of the water column composite photosynthesis-irradiance relationship Figure 4). With the assumption that a single set of parameters was representative, the spatial and temporal patterns in modeled distributions of primary production were primarily driven by patterns in in situ fluorescence, a variable determined with relatively high resolution and precision. To determine the sensitivity of model output to potential errors in parameters, we introduced a variation of ±20% in individual terms and examined the effect on the modeled estimates of water-column-integrated primary production at four representative stations (stations 9, 12, 58, and 59). The range of ±20% was chosen as an approximation of the uncertainty of model estimates of these terms resulting from spatial and temporal variation within the study region (for example, the mean percent deviation between the modeled Chl *a* term and measured values was 20% in the upper 200 m, the depth range applicable for estimating primary production). Results were similar for all four stations (Table 2). The analysis made it evident that model output was most sensitive to errors in estimation of Chl *a*, matching the variation of ±20%. The model was slightly less sensitive to errors in α and P^B_{max}, with output varying by 8–12%. Neither regional nor temporal gradients in the parameters for estimating Chl *a* from fluorescence or the water column composite values of α and P^B_{max} could account for the observed patterns in modeled primary production distributions. There was an apparent temporal dependence in the relationship of total pigments to in situ fluorescence, as evidenced by differences between leg 1 and leg 2 (Figure 1). However, model output was least sensitive to variations in the pigment term (Table 2), such that the use of a common set of pigment parameters for both leg 1 and leg 2 was unlikely to alter our interpretations (in fact, if pigment parameters specific to leg 1 and leg 2 had been used, existing temporal differences in primary production distributions would have been more pronounced).

DISCUSSION

The hypothesis that differences in photosynthetic parameters of phytoplankton populations were related to different physical regimes within the meander and associated water masses was partially supported by our data. Photosynthesis-

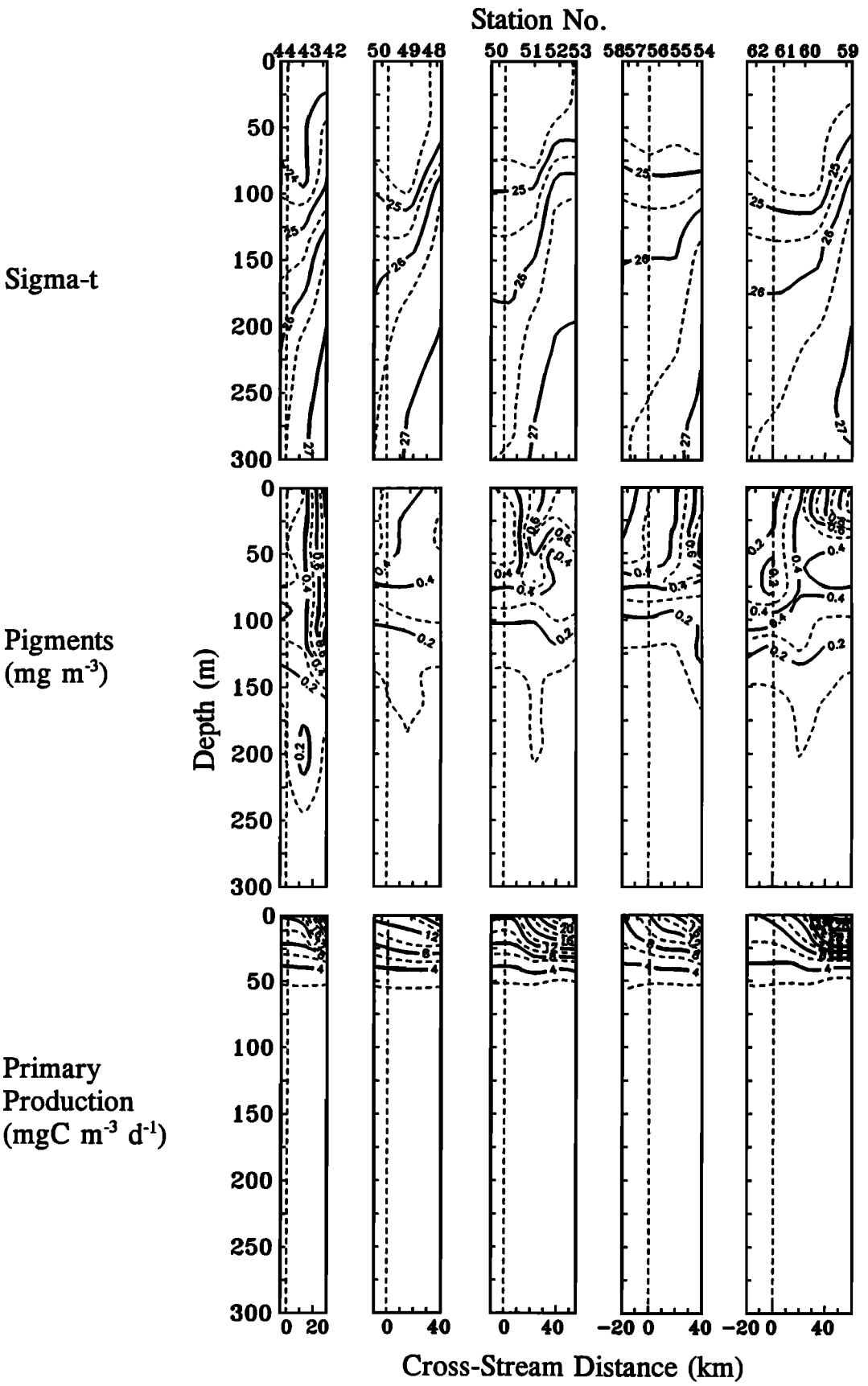

Fig. 9. The σ_t, total pigments, and daily primary production for sections across the Gulf Stream during the leg 2 mesoscale survey. Labeling and notation are as in Figure 7. See Plate 2 for position of transects in relation to meander.

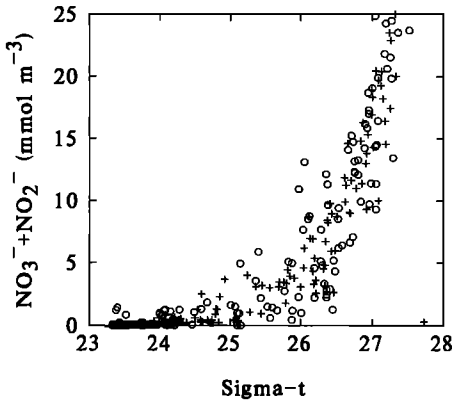

Fig. 10. Relationship of $NO_3^- + NO_2^-$ concentrations to σ_t. Open circles, leg 1; crosses, leg 2.

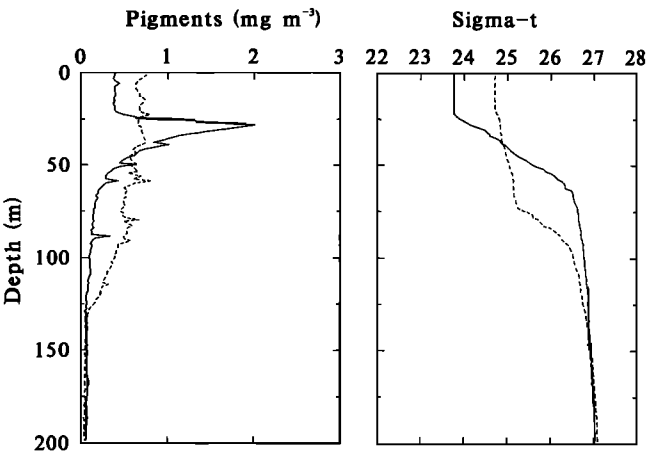

Fig. 11. Vertical profiles of pigments and density at stations 8 (solid line) and 46 (dashed line), occupied during leg 1 and leg 2, respectively, and having similar positions relative to the meander (i.e., similar curvilinear coordinates, see Table 1). Pigment concentrations were estimated from in situ fluorescence profiles and equation (3).

irradiance (*P-I*) parameters of individual samples determined during leg 2 did show spatial variation (Figure 3). Values of α and P^B_{max} in the upper mixed layer ranged higher in the slope water, and this was suggestive of enhancement due to increased nutrient availability [cf. *Falkowski et al.*, 1991; *Platt et al.*, 1992]. Both α and p^B_{max} also displayed a depth dependence (Figure 3). Despite these spatial variations, water column composite *P-I* relationships for each leg were well represented by a single curve (Figure 4). Furthermore, there were no significant differences between leg 1 and leg 2 water column composite *P-I* parameters (Figure 4). This was in spite of the fact that different methods were used to measure primary production. An implication of these findings was that variations in the amount and vertical distribution of photosynthetic pigments had a greater influence on water-column-integrated production than did regional or temporal variations in photosynthetic parameters. A similar observation was reported for phytoplankton populations associated with a frontal boundary in the California Current [*Gaxiola-Castro and Alvarez-Borrego*, 1991].

Our second hypothesis, that along-stream variations in distributions of pigments and primary production could be related to meander physical structure, was also supported by our observations. Distribution patterns were consistent with physical descriptions of Gulf Stream meanders [*Olson*, 1990]. The major evidence for a circulation-induced response was the correspondence of variations in the depths of pigment maxima and isopycnal surfaces along the stream core. During leg 1 (Figure 7), elevated isopycnal surfaces and associated pigment maxima were suggestive of upwelling at the meander crest (stations 2–6). In contrast, depression of isopycnal surfaces and associated pigment maxima were consistent with downwelling in the trough (stations 20–22). During leg 2 (Figure 9) there was similar evidence of vertical shifts in pigment distributions and isopycnal surfaces as a function of position along the meander, although the magnitude of displacement was less than that observed during leg 1. This presumably reflected the characteristics of a more zonal stream during leg 2. Our results confirmed reports by other investigators [*Hitchcock et al.*, 1993] that vertical pigment distributions can be related to physical processes within meanders [*Bower and Rossby*, 1989]. Clearly, pigment distributions must be viewed as the result of a combination of rate processes including physical transport, photoadaptation, in situ growth coupled with nutrient supply, and removal by grazers and sinking. The importance of advective transport was particularly evident in the case of some deep pigment features we observed. For example, the subsurface pigment maximum at station 21 (Figure 7) was apparently advected from shallower waters rather than originating in situ because irradiance was insufficient (0.01–0.03% of surface incident irradiance) for substantial growth at those depths. Further evidence of advection was the fact that TS characteristics at the depth of the subsurface pigment maximum at station 21 were similar to those at the depth of a shallower pigment maximum at the adjacent station 20 (data not shown).

As is apparent in the distributions of pigments, along-stream variations in vertical distributions of primary production were related to meander circulation features. During leg 1, strong cross-stream gradients in rates of primary production were observed at the western transect (stations 2–6) and were less pronounced for subsequent transects downstream (Figure 7). The rates of primary production were apparently related to the depths of the nitracline, with higher rates corresponding to shallower nitracline depths (Figure 8); this was evidence of close coupling between primary production and entrainment of nutrients from deeper waters [*Pelegrí and Csanady*, 1991]. During leg 2, cross-stream gradients in rates of primary production were observed, but along-stream variation was not clearly associated with meander features; this may have been a consequence of the fact that the amplitude of the meander had decreased.

The dominant feature in areal distributions of water-column-integrated pigments and primary production in each of the surveys was the consistently higher values on the slope water side of the stream (Figures 12 and 13) [cf. *Yentsch*, 1974]. Despite the marked influence of the meander on the vertical distribution of pigments, the along-stream variation in water-column-integrated pigment biomass seemed to be secondary within either survey. Note that downstream of the meander crest during leg 1, the deeper distribution of pigments north of the stream front resulted in a less pronounced cross-stream gradient in water-column-integrated primary production (Figure 13); this effect was

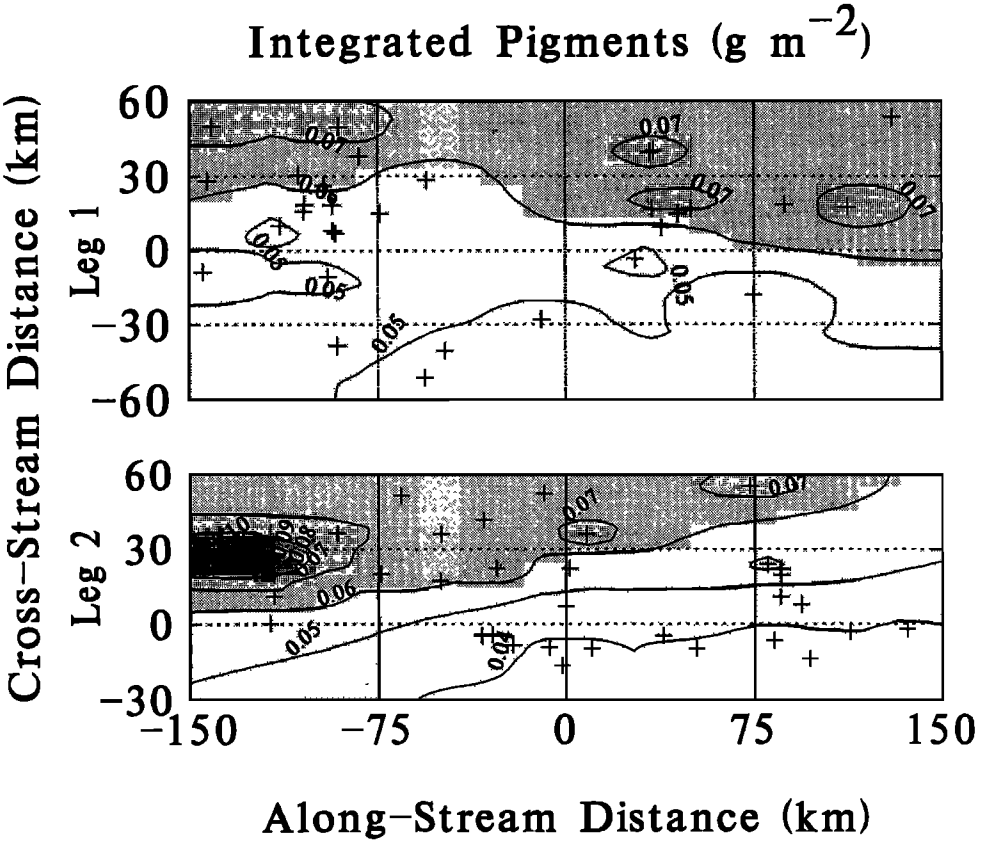

Fig. 12. Areal contour map of water-column-integrated total pigments plotted in a curvilinear coordinate system as described in Figure 3.

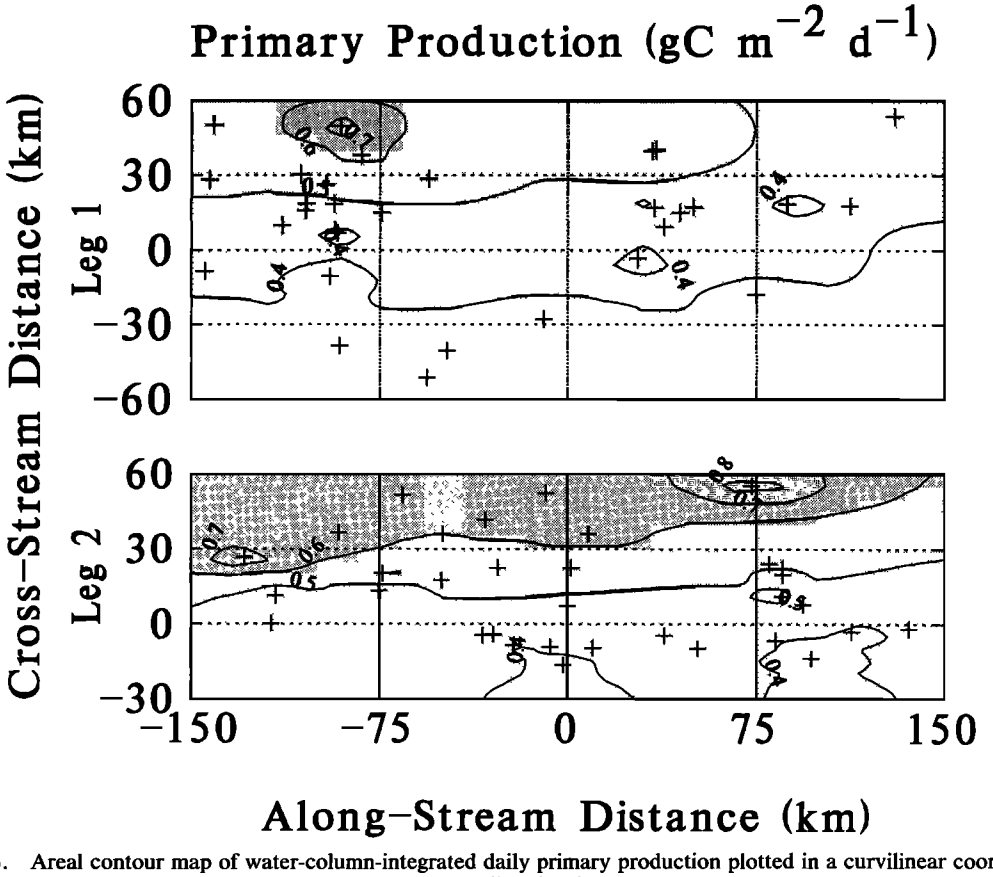

Fig. 13. Areal contour map of water-column-integrated daily primary production plotted in a curvilinear coordinate system as described in Figure 3.

TABLE 2. Sensitivity of Model Output to Variations in Selected Terms at Representative Stations

Term	Station	Change in Integrated Primary Production due to Variation in Terms of +20%	−20%
Total pigments	9	−6	8
	12	−4	4
	58	−3	4
	59	−5	6
Chl *a*	9	20	−20
	12	20	−20
	58	20	−20
	59	20	−20
α	9	11	−12
	12	10	−12
	58	10	−12
	59	9	−11
P^B_{max}	9	8	−10
	12	9	−10
	58	8	−10
	59	9	−11

also apparent in the vertical distributions of primary production (Figure 7). Another feature of our observations was the increase from leg 1 to leg 2 in water-column-integrated production along the northern edge of the front (Figure 13). The increased production without a concurrent change in pigments (Figure 12) was suggestive of mixing-induced nutrient injection; this was in contrast to vertical shifting of populations with their ambient nutrients in the irradiance field as seemed to be the case along the meander during the leg 1 survey.

Speculation that nutrient entrainment into surface waters occurred between leg 1 and leg 2 was supported by the observation of higher surface densities during leg 2 (compare Figures 7 and 9) and the close relationship between density and $NO_3^- + NO_2^-$ concentrations (Figure 10). Further evidence that mixing had occurred was an apparent "erosion" of pigment maxima in the period between leg 1 and leg 2 (Figures 7, 9, and 11) and the lack of any vertical gradient in α in the slope water during leg 2 (Figure 3). There are two basic mechanisms that could be invoked to account for the observed changes in water column structure between leg 1 and leg 2. One possibility was the occurrence of a "fall bloom" in the slope water in response to the observed passage of an atmospheric front. Alternatively, the collapse of the meander and the product of the mixing induced by the ring interaction and the frontogenesis associated with the formation of the zonal Stream might be implicated.

Enhancement of phytoplankton biomass and productivity due to upward entrainment and isopycnal advection of nutrients at deep oceanic current boundary fronts has been suggested [*Yentsch*, 1974; *Fasham et al.*, 1985; *Csanady and Hamilton*, 1988; *Lohrenz et al.*, 1988; *Yentsch and Phinney*, 1991; *Hitchcock et al.*, 1993]. There is evidence to suggest that meanders play an important role in contributing to entrainment and isopycnal advection of nutrients [*Pelegrí and Csanady*, 1991]. Our results have provided an illustration of relationships between mesoscale and fine scale variations at the Gulf Stream current boundary and distributions of pigments and primary production. Meander-induced transport of nutrients may significantly modify the proportion of total primary production supported by exogenous nutrient inputs (i.e., "new production" as defined by *Dugdale and Goering* [1967]). If so, a shift in the importance of nutrient recycling would be expected along a meandering Gulf Stream. This may be manifested in the composition and activities of the microbial communities. Another way in which meander circulation may have significant biological impact is through the transport and exchange among biological communities bordering the Gulf Stream. *Bower and Rossby* [1989] and *Dutkiewicz et al.* [1993] demonstrated cross-frontal exchange related to meander circulation. Such exchange may play an important role in maintaining slope water and Sargasso Sea species distributions. Additional investigation is required to address the significance of these and other factors such as seasonal changes in water mass characteristics.

Acknowledgments. We are grateful for the collaboration of a number of individuals. J. Napp, C. D. Taylor, P. Ortner, and H. L. MacIntyre cooperated in sampling and analyses. C. Flagg, A. J. Mariano, and X. Chen provided helpful information. Thanks to G. Sammuels for AVHRR analysis. Bigelow Laboratories graciously provided the nutrient analyses. Thanks also to the captain and crew of the R/V *Cape Hatteras*. Funding for this research was provided by Office of Naval Research contracts N00014-88-K-0155 (S.E.L.), N00014-90-J1981 (D.A.P. and C.S.Y.), N00014-87K-0311 and N00014-89-J1066 (J.J.C.), and N00014-87-J-1536 and N00014-89-J0116 (D.B.O.), as well as by the Department of Energy (DE-FG02-92ER61443 to S.E.L.). We are also grateful for facilities and equipment provided by the Naval Research Laboratory at Stennis Space Center, Mississippi. This is contribution 164 from the University of Southern Mississippi Center for Marine Science.

REFERENCES

Atkinson, L. P., Modes of Gulf Stream intrusion into South Atlantic Bight shelf waters, *Geophys. Res. Lett.*, *4*, 583–586, 1977.

Bower, A. S., and T. Rossby, Evidence of cross-frontal exchange processes in the Gulf Stream based on isopycnal float data, *J. Phys. Oceanogr.*, *19*, 1177–1190, 1989.

Csanady, G. T., and P. Hamilton, Circulation of slopewater, *Cont. Shelf Res.*, *8*, 565–624, 1988.

Cullen, J. J., X. Yang, and H. L. MacIntyre, Nutrient limitation of marine photosynthesis, in *Primary Productivity and Biogeochemical Cycles in the Sea*, edited by P. G. Falkowski and A. Woodhead, pp. 69–88, Plenum, New York, 1992.

Dugdale, R. C., and J. J. Goering, Uptake of new and regenerated forms of nitrogen in primary productivity, *Limnol. Oceanogr.*, *12*, 196–206, 1967.

Dutkiewicz, S., A. Griffia, and D. Olson, Turbulent diffusion in a meandering jet, *J. Geophys. Res.*, in press, 1993.

Falkowski, P. G., D. Ziemann, Z. Kolber, and P. K. Bienfang, Role of eddy pumping in enhancing primary production in the ocean, *Nature*, *352*, 55–58, 1991.

Fasham, M. J. R., T. Platt, B. Irwin, and K. Jones, Factors affecting the spatial pattern of the deep chlorophyll maximum in the region of the Azores front, *Prog. Oceanogr.*, *14*, 129–165, 1985.

Fee, E. J., Modelling primary production in water bodies: A numerical approach that allows for vertical inhomogeneities, *J. Fish Res. Board Can.*, *30*, 1469–1473, 1973.

Flierl, G. R., and C. S. Davis, Biological effects of Gulf Stream meandering, in SYNOPtician, *Newsl.*, *2*(1), pp. 5–7, Univ. of R.I., Grad. School of Oceanogr., Kingston, 1991.

Fryxell, G. A., R. W. Gould, Jr., E. R. Balmori, and E. C. Theriot, Gulf Stream warm core rings: Phytoplankton in two fall rings of different ages, *J. Plankton Res.*, *7*, 339–364, 1985.

Garside, C., A chemiluminescent technique for the determination of nanomolar concentrations of nitrate and nitrite in seawater, *Mar. Chem.*, *11*, 159–167, 1982.

Gaxiola-Castro, G., and S. Alvarez-Borrego, Relative assimilation

numbers of phytoplankton across a seasonally recurring front in the California Current off Ensenada, *CalCOFI Rep.*, *32*, pp. 91–96, Calif. Coop. Oceanic Fish. Invest., Scripps Inst. of Oceanogr., Univ. of Calif., San Diego, La Jolla, 1991.

Gould, R. W., and G. A. Fryxell, Phytoplankton species composition and abundance in a Gulf Stream warm-core ring, I, Changes over a five month period, *J. Mar. Res.*, *46*, 367–398, 1988.

Gregg, W. W., and K. L. Carder, A simple spectral solar irradiance model for cloudless maritime atmospheres, *Limnol. Oceanogr.*, *35*, 1657–1675, 1990.

Harrison, W. G., T. Platt, and M. R. Lewis, The utility of light-saturation models for estimating marine primary productivity in the field: A comparison with conventional "simulated" in situ methods, *Can. J. Fish. Aquat. Sci.*, *4*, 864–872, 1985.

Hitchcock, G., C. Langdon, and T. J. Smayda, Short-term changes in the biology of a Gulf Stream warm-core ring: Phytoplankton biomass and productivity, *Limnol. Oceanogr.*, *32*, 919–929, 1987.

Hitchcock, G. L., A. J. Mariano, and T. Rossby, Mesoscale pigment fields in the Gulf Stream: Observations in a meander crest and trough, *J. Geophys. Res.*, *98*, 8425–8445, 1993.

Holm-Hansen, O., C. J. Lorenzen, R. W. Holmes, and J.D.H. Strickland, Fluorometric determination of chlorophyll, *J. Cons. Cons. Int. Explor. Mer.*, *30*, 3–15, 1965.

Kirk, J.T.O., *Light and Photosynthesis in Aquatic Ecosystems*, 401 pp., Cambridge University Press, New York, 1983.

Lean, D.R.S., and B.K. Burnison, An evaluation of errors in the ^{14}C method of primary production measurements, *Limnol. Oceanogr.*, *24*, 917–938, 1979.

Lee, T. N., L. P. Atkinson, and R. Legeckis, Observations of a Gulf Stream frontal eddy on the Georgia continental shelf, April 1977, *Deep Sea Res., Part A*, *28*, 347–378, 1981.

Lee, T. N., J. A. Yoder, and L. P. Atkinson, Gulf Stream frontal eddy influence on productivity of the southeast U.S. continental shelf, *J. Geophys. Res.*, *96*, 22,191–22,205, 1991.

Lewis, M. R., and J. C. Smith, A small volume, short-incubation-time method for measurement of photosynthesis as a function of incident irradiance, *Mar. Ecol. Prog. Ser.*, *13*, 99–102, 1983.

Lohrenz, S. E., Estimation of primary production by the simulated in situ method, *Coop. Res. Rep. Int. Counc. Explor. Sea*, in press, 1993.

Lohrenz, S. E., D. A. Wiesenburg, I. P. DePalma, K. A. Johnson, and D. R. Gustafson, Jr., Interrelationships among primary production, chlorophyll and environmental conditions in frontal regions of the western Mediterranean Sea, *Deep Sea Res., Part A*, *35*, 793–810, 1988.

Lohrenz, S. E., D. A. Wiesenburg, C. R. Rein, R. A. Arnone, C. D. Taylor, G. A. Knauer, and A. H. Knap, A comparison of in situ and simulated in situ methods for estimating oceanic primary production, *J. Plankton Res.*, *14*, 201–221, 1992.

Mariano, A. J., Contour analysis: A new approach for melding geophysical fields, *J. Atmos. Oceanic Technol.*, *7*, 285–295, 1990.

Mariano, A. J., Empirical orthogonal contours, in SYNOPtician, *Newsl.*, *2*(4), pp. 6–7, Univ. of R.I., Grad. School of Oceanogr., Kingston, 1991.

McCarthy, J. J., and J. L. Nevins, Sources of nitrogen for primary production in warm-core rings 79-E and 81-D, *Limnol. Oceanogr.*, *31*, 690–700, 1986.

Nelson, D. M., et al., Distribution and composition of biogenic particulate matter in a Gulf Stream warm-core ring, *Deep Sea Res., Part A*, *32*, 1347–1369, 1985.

Olson, D. B., BIOSYNOP: Biophysical studies of Gulf Stream meanders, in SYNOPtician, *Newsl.*, *1*(3), pp. 1–3, Univ. of R.I., Grad. School of Oceanogr., Kingston, 1990.

Ortner, P. B., P. H. Wiebe, L. Haury, and S. Boyd, Variability in biomass distribution in the northern Sargasso Sea: The contribution of Gulf Stream cold core rings, *Fish. Bull.*, *76*, 323–334, 1978.

Parsons, T. R., Y. Maita, and C. M. Lalli, *A Manual of Chemical and Biological Methods for Seawater Analysis*, 173 pp., Pergamon, New York, 1984.

Pelegrí, J. L., and G. T. Csanady, Nutrient transport and mixing in the Gulf Stream, *J. Geophys. Res.*, *96*, 2577–2583, 1991.

Platt, T., C. L. Gallegos, and W. G. Harrison, Photoinhibition of photosynthesis in natural assemblages of marine phytoplankton, *J. Mar. Res.*, *38*, 687–701, 1980.

Platt, T., S. Sathyendranath, O. Ulloa, W. G. Harrison, N. Hoepffner, and J. Goes, Nutrient control of phytoplankton photosynthesis in the western North Atlantic, *Nature*, *356*, 229–231, 1992.

Prieur, L., and S. Sathyendranath, An optical classification of coastal and oceanic waters based on the specific absorption curves of phytoplankton pigments, dissolved organic matter, and other particulate materials, *Limnol. Oceanogr.*, *26*, 671–690, 1981.

Sathyendranath, S., and T. Platt, The spectral irradiance field at the surface and in the interior of the ocean: A model for applications in oceanography and remote sensing, *J. Geophys. Res.*, *93*, 9270–9280, 1988.

Smith, R. C., and K. S. Baker, Spatial and temporal patterns in pigment biomass in Gulf Stream warm-core ring 82B and its environs, *J. Geophys. Res.*, *90*, 8859–8870, 1985.

Taylor, C. D., and K. W. Doherty, Submersible incubation device (SID), autonomous instrumentation for the in situ measurement of primary production and other microbial rate processes, *Deep Sea Res., Part A*, *37*, 343–358, 1990.

The Ring Group, Gulf Stream cold-core rings: Their physics, chemistry, and biology, *Science*, *212*, 1091–1100, 1981.

Tracey, K., and R. Watts, Vignette #1: Will this meander trough pinch off? in SYNOPtician, *Newsl.*, *2*(2), pp. 9–10, Univ. of R.I., Grad. School of Oceanogr., Kingston, 1990.

Van Heuklon, T. K., Estimating atmospheric ozone for solar radiation models, *Sol. Energy*, *22*, 63–68, 1979.

Whitledge, T. E., S. C. Malloy, C. J. Patton, and C. D. Wirick, Automated nutrient analysis in seawater, *Formal Rep. 51398*, 216 pp., Brookhaven Natl. Lab., Upton, N. Y., 1981.

Yentsch, C. S., The influence of geostrophy on primary production, *Tethys*, *6*, 111–118, 1974.

Yentsch, C. S., and D. A. Phinney, Wind forcing and inertial processes: A comparative view of the level of productivity generated by western boundary currents, in SYNOPtician, *Newsl.*, *2*(1), pp. 4–5, Univ. of R.I., Grad. School of Oceanogr., Kingston, 1991.

Yoder, J. A., L. A. Atkinson, S. S. Bishop, J. O. Blanton, T. N. Lee, and L. J. Pietrafesa, Phytoplankton dynamics within Gulf Stream intrusions on the southeastern United States continental shelf during summer 1981, *Cont. Shelf Res.*, *4*, 611–635, 1985.

J. J. Cullen, Department of Oceanography, Dalhousie University, Halifax, Nova Scotia, Canada B3H 4J1.

Steven E. Lohrenz, Center for Marine Science, University of Southern Mississippi, Stennis Space Center, MS 39529.

D. B. Olson, Rosenstiel School of Marine and Atmospheric Sciences, University of Miami, 4600 Rickenbacker Causeway, Miami, FL 33149.

D. A. Phinney, and C. S. Yentsch, Bigelow Laboratory for Ocean Sciences, West Boothbay Harbor, ME 04575.

(Received September 16, 1992;
revised February 23, 1993;
accepted March 15, 1993.)